Chinese Chemical Letters 34 (2023) 107251

Contents lists available at ScienceDirect

Chinese Chemical Letters

journal homepage: www.elsevier.com/locate/cclet

A series of heterometallic 3d-4f polyoxometalates as single-molecule magnets

Shurong Li[a], Zhenzhang Weng[a], Linpeng Jiang[a], Rongjia Wei[b], Haifeng Su[a], Lasheng Long[a], Lansun Zheng[a], Xiangjian Kong[a,*]

[a] Collaborative Innovation Center of Chemistry for Energy Materials, State Key Laboratory of Physical Chemistry of Solid Surfaces and Department of Chemistry, College of Chemistry and Chemical Engineering, Xiamen University, Xiamen 361005, China
[b] College of Chemistry and Materials Science, Jinan University, Guangzhou 510632, China

ARTICLE INFO

Article history:
Received 26 January 2022
Revised 16 February 2022
Accepted 21 February 2022
Available online 24 February 2022

Keywords:
Polyoxometalates
3d-4f
Cluster
Lanthanide
Single-molecule magnet

ABSTRACT

Three sandwich-like $[Ln_2Fe_2(B\text{-}\alpha\text{-}FeW_9O_{34})_2]^{10-}$ clusters (Ln_2Fe_4, Ln = Dy (**1**), Ho (**2**), and Y (**3**)) were obtained by reacting $Na_9[B\text{-}\alpha\text{-}SbW_9O_{33}]$, Ln_2O_3, $FeCl_3{\cdot}6H_2O$ and KH_2PO_4. The $[B\text{-}\alpha\text{-}FeW_9O_{34}]^{11-}$ units were formed *via* the *in situ* conversion of lacunary polyoxometalates (POM) $[B\text{-}\alpha\text{-}SbW_9O_{33}]^{9-}$ and the Ln^{3+} ions were generated from the slow dissolution of Ln_2O_3, both of which play important roles in the synthesis of Ln_2Fe_4. Ln_2Fe_4 is the first 3d-4f cluster assembled from d-metal heteroatom-containing POM. The Dy_2Fe_4 cluster exhibits single-molecule magnet properties with an 80 K energy barrier in an optimal DC field. Cyclic voltammetry tests and controlled-potential coulometry experiments show that the polyoxometalate Fe heteroatom in clusters **1–3** is also electrochemically active.

Heterometallic 3d-4f cluster compounds have attracted widespread interest due to their interesting optical, electrical, magnetic, and catalytic properties resulting from the contribution of 3d and 4f electrons [1–9]. Considerable efforts in this field have resulted in the fabrication of a large number of 3d-4f clusters with fascinating structures, and unique physical and chemical properties based on various organic ligands. In these clusters, the organic ligands play an important protecting and bridging role in the separation and preparation of cluster structures [10–12]. 3d-4f Clusters protected by inorganic ligands have higher thermal stabilities and unique rigid structures compared to 3d-4f clusters protected by organic ligands [13,14].

Lacunary polyoxometalates (POMs) are a class of inorganic multidentate ligands with well-defined vacant sites and high negative charges. These are commonly used to prepare stable metal oxygen clusters or cluster-of-cluster aggregates due to their high nucleophilicity and high reactivity [15–19]. Several 3d metal clusters based on the trivacant POM $\{XW_9O_{34}\}$ (heteroatom x = P, Si, Sb) have been reported [20–29]. However, the synthesis of POM-based 3d-4f clusters remains challenging due to the coordination competition between 3d metal ions and 4f ions in inorganic POM ligands. Moreover, the strong reaction between 4f ions and the oxygen-rich POM makes precipitation easy but crystallization difficult [13,14,30–34]. Therefore, reducing the reaction rate of lanthanide ions with POMs may be an effective strategy for the synthesis of POM-based 3d-4f clusters [35–37]. In this study, we have obtained three $\{FeW_9O_{34}\}$-based 3d-4f clusters, formulated—$Na_8K_2[Fe_2Ln_2(H_2O)_4(B\text{-}\alpha\text{-}FeW_9O_{34})_2]{\cdot}nH_2O$ (Ln_2Fe_4, where Ln = Dy and n = 17 for cluster **1**; Ln = Ho and n = 15 for cluster **2**; and Ln = Y and n = 14 for cluster **3**). These clusters have classical sandwich-type structures, where the $[(B\text{-}\alpha\text{-}FeW_9O_{34})^{11-}]$ unit is generated *via* the transformation of the $[(B\text{-}\alpha\text{-}SbW_9O_{33})^{9-}]$ precursor (Figs. 1a and b). Ln_2Fe_4 is the first 3d-4f cluster assembled from POMs containing d-metal heteroatoms. Interestingly, Dy_2Fe_4 exhibits single-molecule magnet (SMM) behavior with a high energy barrier.

Clusters **1–3** were synthesized from $Na_9[B\text{-}\alpha\text{-}SbW_9O_{33}]{\cdot}19.5H_2O$, Ln_2O_3 (Ln = Dy/Ho/Y), $FeCl_3{\cdot}6H_2O$ and KH_2PO_4 under hydrothermal conditions (details in Supporting information). Single-crystal X-ray diffraction analysis showed that the isomorphic clusters **1–3** crystallized in the triclinic crystal system with a *P*-1 space groups (Table S1 in Supporting information). The valence bonding theory calculations of the three clusters (Tables S2-S4 in Supporting information) and the Mössbauer spectrum of cluster **3** indicate that the Fe ions are all high-spin Fe^{3+} (Fig. S3, Tables S5 and S6 in Supporting information) [38]. As shown in Figs. 1c and d, anion cluster **1** $[(B\text{-}\alpha\text{-}FeW_9O_{34})_2Fe_2Dy_2(H_2O)_4]^{10-}$ exhibits a classic sandwich structural unit, which can be observed

* Corresponding author.
E-mail address: xjkong@xmu.edu.cn (X. Kong).

https://doi.org/10.1016/j.cclet.2022.02.056
1001-8417/

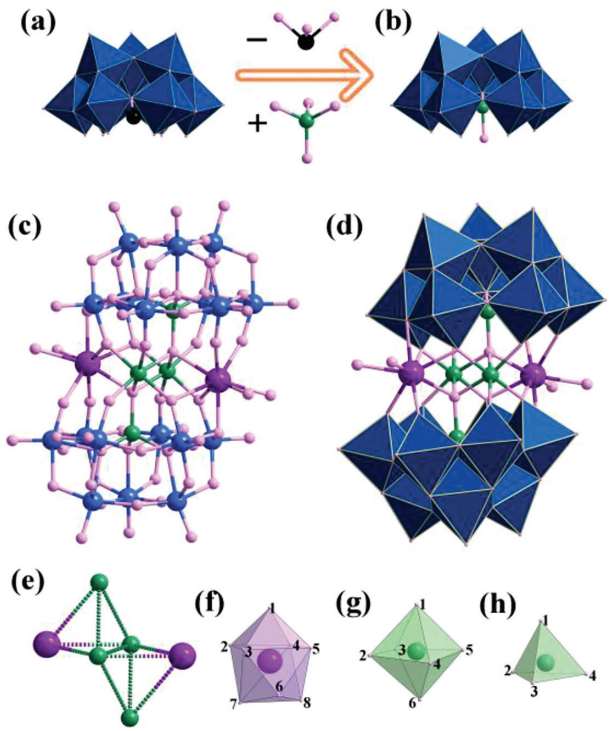

Fig. 1. The structures of (a) $[B\text{-}\alpha\text{-}SbW_9O_{33}]^{9-}$ unit; (b) $[B\text{-}\alpha\text{-}FeW_9O_{34}]^{11-}$ unit. (c, d) Ball-and-stick/polyhedral view of $[(B\text{-}\alpha\text{-}FeW_9O_{34})_2Fe_2Dy_2(H_2O)_4]^{10-}$. (e) The metal core of $2Dy^{3+}$ and $4Fe^{3+}$ ions in cluster **1**. (f-h) The coordination geometries of $DyO_8/FeO_6/FeO_4$. Color key: W/WO_6, blue; $Fe/FeO_6/FeO_4$, green; Dy/DyO_8, purple; Sb, black and O, pink.

as a $[Fe_2Dy_2(H_2O)_4]^{12+}$ unit sandwiched by two inorganic $[(B\text{-}\alpha\text{-}FeW_9O_{34})^{11-}]$ ligands. The $[(B\text{-}\alpha\text{-}FeW_9O_{34})^{11-}]$ unit is formed *via* the *in situ* transformation of the $[(B\text{-}\alpha\text{-}SbW_9O_{33})^{9-}]$ precursor. The Ln_2Fe_4 described in this study is the first 3d-4f cluster containing a trilacunary $[(B\text{-}\alpha\text{-}FeW_9O_{34})^{11-}]$ unit [39–43]. The formation of the $[(B\text{-}\alpha\text{-}FeW_9O_{34})^{11-}]$ species was investigated using single-crystal structure analysis, infrared spectroscopy, and energy dispersive spectroscopy (Figs. S1, S4-S6 in Supporting information). The metal core Fe_4Dy_2 in cluster **1** has exactly two tetrahedral structures with shared edges, with Fe···Fe distances of 3.1301(33)–3.3196(29) Å and Fe···Dy distances of 3.4987(22)–3.7597(26) Å (Fig. 1e, Fig. S18 and Table S12 in Supporting information). Continuous shape measurement (CShM) using Alvarez's SHAPE program (Table S8 in Supporting information) [44,45] shows that Dy^{3+} in the $[Fe_2Dy_2(H_2O)_4]^{12+}$ unit is 8-coordinated with triangular dodecahedral geometry (Fig. 1f), which is different from that reported for Fe_4Dy_2 [46–50]. The Dy-O length is between 2.243(12) Å and 2.514(15) Å (Table S7 in Supporting information). Six-coordinated Fe^{3+} has a classical octahedral geometry (Fig. 1g) with an Fe-O length of 1.991(10) Å–2.048(10) Å, whereas 4-coordinated Fe^{3+} in $[(FeW_9O_{34})^{11-}]$ has a special tetrahedral geometry (Fig. 1h) with an Fe-O length of 1.834(10) Å–1.856(10) Å (Table S2). Clusters **2** and **3** have the same coordination pattern and similar bond lengths and bond angles as cluster **1** (Tables S3, S4, S7 and S8 in Supporting information). Based on elemental analysis, thermogravimetric analysis (Fig. S2 in Supporting information), ion chromatography, and charge balance theory, there are 8 Na^+ and 2 K^+ counter cations. As shown in Figs. S7 and S8 (Supporting information), the $[(B\text{-}\alpha\text{-}FeW_9O_{34})_2Fe_2Dy_2]^{10-}$ anions are connected through hydrated Na^+ and K^+ counter ions to form a two-dimensional framework. The minimum asymmetric units of clusters **1-3** are shown in Figs. S9-S11 (Supporting information).

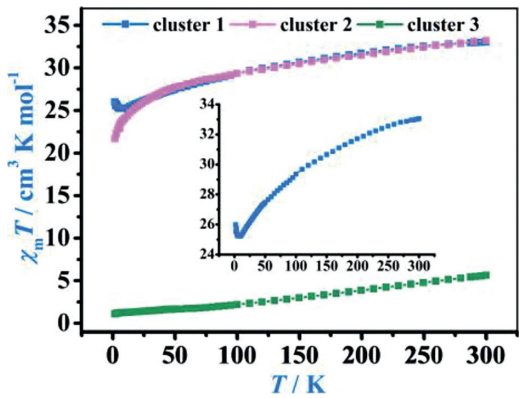

Fig. 2. $\chi_m T$ *vs.* T in the range of 2–300 K under an applied field of 1000 Oe for clusters **1**–**3**. Inset: Enlarged view of the upturn of $\chi_m T$ (cluster **1**).

The use of insoluble lanthanide substances also plays a key role in the formation of clusters **1**–**3**. Clusters **1–3** can be obtained using insoluble lanthanide salts such as $Ln_2(CO_3)_3$ and $Ln_2(SO_4)_3$ to replace Ln_2O_3 (Ln = Dy, Ho and Y). However, such clusters cannot be obtained using soluble $LnCl_3$ or $Ln(NO_3)_3$ salts. Ln_2O_3 can slowly release Ln^{3+} ions under mild acidic conditions (pH 5.5) and medium-high temperature hydrothermal conditions (140 °C). The low equilibrium concentration of Ln^{3+} ions during the reaction can effectively slow the reaction rate between Ln^{3+} and POMs to prevent precipitation. Therefore, combining *in situ* POM transformation with the slow release of Ln^{3+} ions might be an effective synthetic strategy for the synthesis of POM-based 3d-4f clusters.

The variable-temperature magnetic susceptibilities ($\chi_m T$) of clusters **1–3** were measured between 2 K and 300 K under a 1000 Oe applied magnetic field. The relevant magnetic data obtained from these measurements are listed in Table S9 (Supporting information). The experimental $\chi_m T$ values for clusters **1–3** at 300 K (33.05, 32.20 and 5.63 cm^3 K/mol, respectively) are smaller than the expected values (45.83, 45.63 and 17.50 cm^3 K/mol, respectively), which may be due to antiferromagnetic interactions in the clusters [51]. As shown in Fig. 2, with decreasing temperature, the $\chi_m T$ values of clusters **2** and **3** gradually decrease to 21.69 cm^3 K/mol and 1.09 cm^3 K/mol at 2 K, respectively, mainly due to the thermal depopulation of the excited states at the m_J sublevels of the Fe^{3+} and Ho^{3+} ions. The $\chi_m T$ values of cluster **1** gradually decreased to 25.22 cm^3 K/mol at 9 K followed by a sudden rebound to 25.99 cm^3 K/mol at 2 K. This indicates that the presence of weak dipole interactions and/or ferromagnetic interactions between Dy^{3+} and Fe^{3+} below 9 K, including the decrease above 9 K can be attributed to the thermal depopulation of the excited states at the m_J sublevels of the Fe^{3+} and Dy^{3+} ions [52]. Fitting the $\chi_m{}^{-1}$-T data individually in the appropriate temperature interval for these three clusters according to the Curie-Weiss law gives C = 34.77 cm^3/mol, $\theta = -17.57$ K (**1**); C = 34.57 cm^3/mol, $\theta = -16.87$ K (**2**); and C = 34.45 cm^3/mol, $\theta = -1554.21$ K (**3**) (Figs. S12-S14 in Supporting information), which further indicates the presence of antiferromagnetic interactions. As shown in Figs. S15-S17 (Supporting information), the inter-cluster magnetic interactions are negligible due to the long distances. Cluster **3** has only Fe-Fe magnetic interactions, whereas cluster **1** (**2**) has Fe-Fe and Fe-Dy (Fe-Ho) magnetic interactions (Fig. S18 in Supporting information). Therefore, the difference in $\chi_m T$ values between isomorphic clusters **1**, **2** and **3** can be attributed to the contribution of Fe-Dy (Fe-Ho) magnetic interactions (Fig. S19 in Supporting information). The field-dependent magnetization curves of **1–3** at 2 K are shown in Fig. S20 (Supporting information). The experimental values at 7 T are much smaller than their theoretical saturation

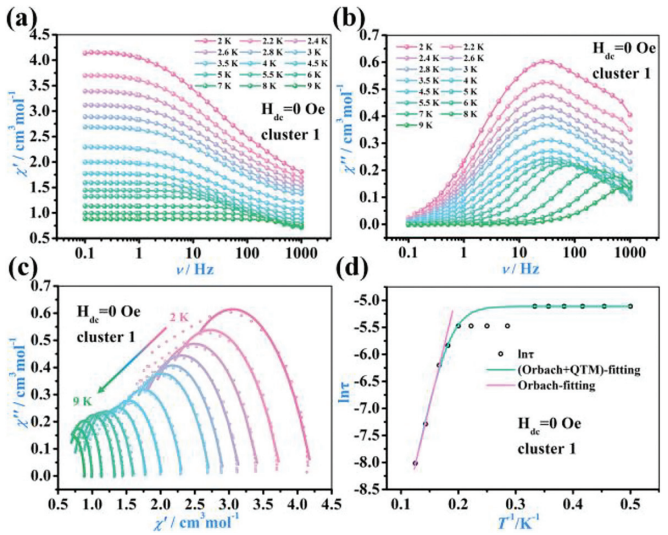

Fig. 3. (a) In-phase susceptibility (χ') and (b) out-of-phase susceptibility (χ'') *vs.* ν under zero Oe DC field for **1**. (c) Cole-Cole plots for AC susceptibilities under zero DC field. The colored solid lines are the best fit to the generalized Debye model. (d) Arrhenius plots of $\ln\tau$ *vs.* T^{-1} for **1** under zero DC field.

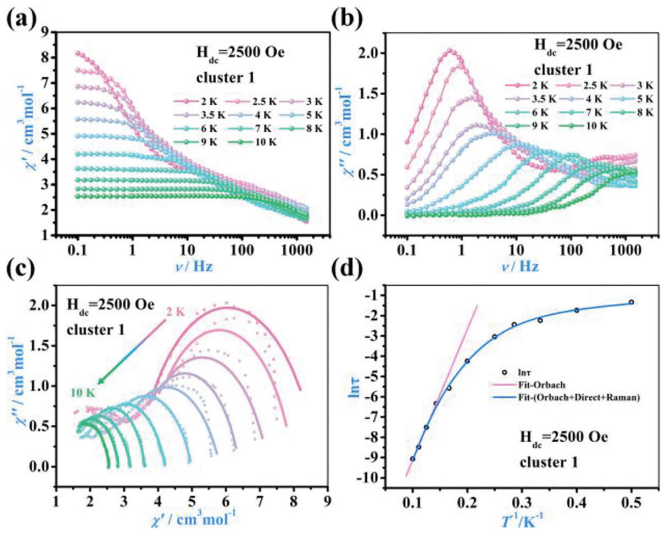

Fig. 4. (a) In-phase (χ') and (b) out-of-phase susceptibility (χ'') *vs.* ν at indicated temperatures under a 2500 Oe DC field for cluster **1**. (c) Cole-Cole plots for AC susceptibilities under a 2500 Oe DC field. The colored solid lines are the best fit to the generalized Debye model. (d) Arrhenius plots of $\ln\tau$ *vs.* T^{-1} for cluster **1**.

values. Furthermore, the *M vs. H/T* curves at different temperatures are not superimposed on a single master curve (Fig. S20, Table S9), which suggests the existence of significant magnetic anisotropy and/or low-lying excited states [53].

AC susceptibility measurements of clusters **1**–**3** were performed to explore their dynamic magnetic properties at indicated frequencies under zero DC field and a 3 Oe AC field at 2 K. As shown in Figs. S21 (Supporting information), the out-of-phase susceptibilities (χ'') of clusters **2** and **3** exhibit temperature dependence at 100–1500 Hz, but no significant peaks are observed due to the quantum tunneling effect. The in-phase susceptibilities (χ') and the out-of-phase susceptibilities (χ'') of cluster **1** exhibit obvious temperature dependence, and the out-of-phase susceptibilities (χ'') have obvious peaks at 0.1–1500 Hz. The AC magnetic susceptibility of cluster **1** was further tested at the specified temperatures in the frequency range of 0.1–1000 Hz under zero DC field and a 3 Oe AC field. Figs. 3a and b show the frequency dependence plots of χ' and χ''. A series of single frequency-dependent peaks were observed between 2 K and 9 K, indicating the SMM behavior of cluster **1**. The Cole-Cole plots were fitted using the generalized Debye model (Fig. 3c). The large α values under zero DC field indicates the presence of multiple relaxation processes (Table S10 in Supporting information) [54]. The $\ln\tau$ *vs.* T^{-1} plots are almost linear when $T > 7$ K, which can be fitted by considering only the Orbach relaxation process using Arrhenius' law ($\tau = \tau_0 \exp(U_{\text{eff}}/k_B T)$). The obtained parameters are $U_{\text{eff}}/k_B =$ 43.68 K and $\tau_0 = 1.4 \times 10^{-6}$ s, which is consistent with the reported ranges for other SMMs (10^{-6}–10^{-11} s). However, when $T < 7$ K, the $\ln\tau$ *vs.* T^{-1} plots deviate from linearity, indicating the presence of other magnetic relaxation processes. Combining the Obrach and quantum tunneling of magnetization (QTM) relaxation processes using the equation $\tau^{-1} = \tau_0{}^{-1} \exp(-U_{eff}/k_B T) + \tau_{\text{QTM}}{}^{-1}$ gives the best fit ($R^2 = 0.99865$), where τ_{QTM} is the rate of QTM. The fit gives $\tau_0 = 6.4 \times 10^{-7}$ s, $\tau_{\text{QTM}} = 6.0 \times 10^{-3}$ s, and U_{eff}/k_B = 50.24 K (Fig. 3d). To slow relaxation, the AC magnetic susceptibilities were measured under specific DC fields at 2 K. Under DC fields from 1000 Oe to 4000 Oe, the out-of-phase AC signal values increased significantly compared to those at 0 Oe (Fig. S22 in Supporting information), indicating that QTM is suppressed. Simultaneously, the frequency corresponding to the peak of the AC signal effectively decreases after applying the field and remains stable above 2500 Oe (Fig. S23 in Supporting information). The AC susceptibilities of cluster **1** were measured under an optimal 2500 Oe DC field. The temperature-dependent and frequency-dependent out-of-phase susceptibilities (χ'') are significantly higher than that at zero field. The peak frequency is lower, and the peak temperature is slightly higher under the same frequency conditions. The Cole-Cole plot obtained by fitting the same generalized Debye model shows a semicircular shape (Fig. 4 and Fig. S24 in Supporting information). Similarly, the $\ln\tau$ *vs.* T^{-1} plot is almost linear in the high-temperature region; considering only the Orbach relaxation process fitted according to Arrhenius' law: $U_{\text{eff}}/k_B = 64.55$ K, and $\tau_0 = 1.7 \times 10^{-7}$ s. In the low-temperature region, the $\ln\tau$ *vs.* T^{-1} plot deviates from linearity. As shown in Fig. 4d, combining the Obrach, direct and Raman relaxation processes using the equation $\tau^{-1} = \tau_0{}^{-1} \exp(-U_{\text{eff}}/k_B T) + AT + CT^n$, results in $\tau_0 = 9.3 \times 10^{-8}$s, $U_{\text{eff}}/k_B = 80.21$ K, A = 1.97 K^{-1} s^{-1}, C = 1.51×10^{-3} s^{-1} K^{-n}, n = 6.6 ($R^2 = 0.99762$). If the QTM relaxation process is also considered, the fitted $\tau_{\text{QTM}} = -8.05 \times 10^{14}$ s, suggesting that QTM can be considered completely suppressed at 2500 Oe [33,55].

POMs are redox reversible and maintain high structural stability while rapidly gaining and losing multiple electrons [56]. The cyclic voltammograms and controlled-potential coulometry experiments showed that the isomorphic clusters **1-3** have three redox processes, peak shapes, and potentials similar to those of the Fe_6W_{18} cluster, which indicates the gradual reduction of the four Fe^{III} centers. Based on the peak reduction currents, the three redox processes are correspond to the two-electron process, the one-electron process and the one-electron process, respectively (Figs. S25 and S26 in Supporting information). Clusters **1-3** are structurally similar to the reported cluster Fe_6W_{18}, which have only two Fe ions replaced by lanthanide ions at the periphery of the sandwich part [43]. Therefore, the Fe heteroatoms in clusters **1–3** (Ln_2Fe_4) can participate in the electrochemical redox process, whereas the Fe heteroatoms in the Fe_6W_{18} cluster are electrochemically inert. Notably, among the POMs containing d-metal heteroatoms, only a few heteroatoms exhibit electrochemical activity [57]. The stability of cluster **1-3** in solution was confirmed by ESI-MS (Figs. S27-S29 in Supporting information).

In summary, three $\{FeW_9O_{34}\}$-based 3d-4f clusters were obtained *via* a strategy that employs the slow release of lanthanide ions. The sandwich-like Ln_2Fe_4 clusters are the first 3d-4f clus-

ters assembled from POMs containing d-metal heteroatoms. The *in situ* formation of [B-α-FeW_9O_{34}]$^{11-}$ and the slow release of Ln^{3+} play important roles in the formation of Ln_2Fe_4. Interestingly, the Dy_2Fe_4 cluster exhibits single molecule magnet properties with an 80 K energy barrier under an optimal DC field. The assembly of lacunary polyoxometalate-based 3d-4f SMMs is currently in progress.

Declaration of competing interest

The authors declare that there is no interest for this manuscript.

Acknowledgments

This work was supported by the National Natural Science Foundation of China (Nos. 21871224, 92161104, 92161203 and 21721001) and Innovation Laboratory for Sciences and Technologies of Energy Materials of Fujian Province (IKKEM No. RD2021040301).

Supplementary materials

Supplementary material associated with this article can be found, in the online version, at doi:10.1016/j.cclet.2022.02.056.

References

[1] L.Z. Cai, Q.S. Chen, C.J. Zhang, et al., J. Am. Chem. Soc. 137 (2015) 10882–10885.
[2] R. Chen, C.L. Chen, M.H. Du, et al., Chem. Commun. 57 (2021) 3611–3614.
[3] R. Chen, Z.H. Yan, X.J. Kong, et al., Angew. Chem. Int. Ed. 57 (2018) 16796–16800.
[4] W.P. Chen, G.J. Zhou, Z.L. Gou, et al., Chin. Chem. Lett. 32 (2021) 838–841.
[5] M.H. Du, S.H. Xu, G.J. Li, et al., Angew. Chem. Int. Ed. 61 (2022) e202116296.
[6] N.F. Li, Q.F. Lin, Y.M. Han, et al., Chin. Chem. Lett. 32 (2021) 3803–3806.
[7] H.J. Lun, M.H. Du, D.H. Wang, et al., Inorg. Chem. 59 (2020) 7900–7904.
[8] X. Wang, M.H. Du, H. Xu, et al., Inorg. Chem. 60 (2021) 5925–5930.
[9] H.L. Zhang, Y.Q. Zhai, L. Qin, et al., Matter 2 (2020) 1481–1493.
[10] R. Chen, Z.F. Hong, Y.R. Zhao, et al., Inorg. Chem. 58 (2019) 15008–15012.
[11] H. Han, Y.S. Ding, X. Zhu, et al., Inorg. Chem. Front. 7 (2020) 4070–4076.
[12] M.G.F. Vaz, M. Andruh, et al., Coord. Chem. Rev. 427 (2021) 213611–213634.
[13] V. Das, R. Kaushik, F. Hussain, Coord. Chem. Rev. 143 (2020) 213271–213291.
[14] J.W. Zhao, Y.Z. Li, L.J. Chen, et al., Chem. Commun. 52 (2016) 4418–4445.
[15] J. Cai, X.Y. Zheng, J. Xie, et al., Inorg. Chem. 56 (2017) 8439–8445.
[16] C. Dey, J. Cluster Sci. 33 (2022) 1839–1856.
[17] C. Li, N. Mizuno, K. Yamaguchi, et al., J. Am. Chem. Soc. 141 (2019) 7687–7692.
[18] J.X. Liu, X.B. Zhang, Y.L. Li, et al., Coord. Chem. Rev. 414 (2020) 213260–213276.
[19] H.Y. Wang, X.Y. Zheng, L.S. Long, et al., Inorg. Chem. 60 (2021) 6790–6795.
[20] B.S. Bassil, M. Ibrahim, R. Al-Oweini, et al., Angew. Chem. Int. Ed. 50 (2011) 5961–5964.
[21] B. Godin, Y.G. Chen, J. Vaissermann, et al., Angew. Chem. Int. Ed. 44 (2005) 3072–3075.
[22] X.B. Han, Y.G. Li, Z.M. Zhang, et al., J. Am. Chem. Soc. 137 (2015) 5486–5493.
[23] X.B. Han, Z.M. Zhang, T. Zhang, et al., J. Am. Chem. Soc. 136 (2014) 5359–5366.
[24] L. Huang, S.S. Wang, J.W. Zhao, et al., J. Am. Chem. Soc. 136 (2014) 7637–7642.
[25] M. Ibrahim, Y. Lan, B.S. Bassil, et al., Angew. Chem. Int. Ed. 50 (2011) 4708–4711.
[26] Z.J. Liu, X.L. Wang, C. Qin, et al., Coord. Chem. Rev. 313 (2016) 94–110.
[27] S.S. Mal, U. Kortz, Angew. Chem. Int. Ed. 44 (2005) 3777–3780.
[28] L. Qiao, M. Song, A. Geng, et al., Chin. Chem. Lett. 30 (2019) 1273–1276.
[29] Y. Sakai, K. Yoza, C.N. Kato, et al., Chem. Eur. J. 9 (2003) 4077–4083.
[30] X. Feng, W. Zhou, Y. Li, et al., Inorg. Chem. 51 (2012) 2722–2724.
[31] M. Ibrahim, V. Mereacre, N. Leblanc, et al., Angew. Chem. Int. Ed. 54 (2015) 15574–15578.
[32] Y.D. Lin, R. Ge, C.B. Tian, et al., Chem. Commun. 57 (2021) 8624–8627.
[33] E. Tanuhadi, E. Al-Sayed, G. Novitchi, et al., Inorg. Chem. 59 (2020) 8461–8467.
[34] Y. Chen, Z.W. Guo, X.X. Li, et al., CCS Chem. 3 (2021) 1232–1241.
[35] S.R. Li, H.Y. Wang, H.F. Su, et al., Small. Methods 5 (2020) 2000777.
[36] H.H. Wu, S. Yao, Z.M. Zhang, et al., Dalton. Trans. 42 (2013) 342–346.
[37] L.L. Li, G.J. Cao, J.W. Zhao, et al., Inorg. Chem. 55 (2016) 5671–5683.
[38] G. Abbas, Y. Lan, V. Mereacre, et al., Inorg. Chem. 48 (2009) 9345–9355.
[39] J. Bai, F. Li, Z. Sun, et al., Inorg. Chim. Acta 458 (2017) 1–7.
[40] D. Barats, G. Leitus, R. Popovitz-Biro, et al., Angew. Chem. Int. Ed. 47 (2008) 9908–9912.
[41] M.P.E.M. Limanski, E. Droste, K. Burgemeister, et al., J. Cluster Sci. 13 (2002) 369–379.
[42] P.T. M, J.P. Wang, Y. Shen, et al., Cryst. Growth. Des. 7 (2007) 603–605.
[43] J.D. Compain, P. Mialane, A. Dolbecq, et al., Angew. Chem. Int. Ed. 48 (2009) 3007–3081.
[44] M. Llunell, D. Casanova, J. Girera, P. Alemany, S. Alvarez, SHAPE, Version 2.0, Shape Software, Barcelona, 2010.
[45] H. Zabrodsky, S. Peleg, D. Avnir, J. Am. Chem. Soc. 115 (1993) 8278–8289.
[46] M.N. Akhtar, V. Mereacre, G. Novitchi, et al., Chem. Eur. J. 15 (2009) 7278–7282.
[47] A. Baniodeh, C.E. Anson, A.K. Powell, Chem. Sci. 4 (2013) 4354–4361.
[48] L.J. Chen, F. Zhang, X. Ma, et al., Dalton 44 (2015) 12598–12612.
[49] S.F.M. Schmidt, C. Koo, V. Mereacre, J. Park, D.W. Heermann, et al., Inorg. Chem. 56 (2017) 4796–4806.
[50] J.J. Jiang, Y.H. Chen, L.L. Liu, et al., Inorg. Chem. 58 (2019) 15853–15863.
[51] X.Y. Zheng, H. Zhang, Z. Wang, et al., Angew. Chem. Int. Ed. 56 (2017) 11475–11479.
[52] G. Peng, Y.Y. Zhang, B. Li, et al., Dalton. Trans. 47 (2018) 17349–17356.
[53] Y. Huo, Y.C. Chen, S.G. Wu, et al., Inorg. Chem. 58 (2019) 1301–1308.
[54] K.C. Mondal, A. Sundt, Y.H. Lan, et al., Angew. Chem. Int. Ed. 51 (2012) 7550–7554.
[55] F. Shao, B. Cahier, Y.T. Wang, et al., Chem. Asian. J. 15 (2020) 391–397.
[56] J.J. Chen, M. Symes, L. Cronin, Nat. Chem. 10 (2018) 1042–1047.
[57] Y.Y. Liu, S.F. Lu, H.N. Wang, Adv. Energy Mater. 7 (2017) 1601224.